Silicon Quantum Dot Supraparticles for Fluorescence Bioimaging

Fujii, Minoru
Fujii, Riku
Takada, Miho
Sugimoto, Hiroshi

(Citation)
ACS Applied Nano Materials,2020(3):6099-6107

(Issue Date)
2020-05-18

(Resource Type)
journal article

(Version)
Accepted Manuscript

(URL)
https://hdl.handle.net/20.500.14094/90009537

Silicon Quantum Dot Supraparticles for Fluorescence Bioimaging

*Minoru Fujii, * Riku Fujii, Miho Takada, and Hiroshi Sugimoto***

Department of Electrical and Electronic Engineering, Graduate School of Engineering, Kobe University, Rokkodai, Nada, Kobe 657-8501, Japan

*fujii@eedept.kobe-u.ac.jp

**sugimoto@eedept.kobe-u.ac.jp

KEYWORDS. supraparticle, silicon, quantum dot, luminescence, near infrared

ABSTRACT. We developed a self-limited self-assembly process to produce red-to-near-infrared luminescent supraparticles made from bio-compatible silicon (Si) quantum dots (QDs) for fluorescence bio-imaging. A starting material is a methanol solution of boron (B) and phosphorus (P) codoped all-inorganic Si QDs. The Si QDs have a heavily B and P codoped amorphous shell and the shell induces negative potential on the surface, which prevents agglomeration of QDs in polar solvents. By adding toluene to the methanol solution, controlled agglomeration of Si QDs occurs and spherical supraparticles around 100 nm in diameter with a narrow size distribution are grown. The average diameter of supraparticles was controlled by the growth parameters. We also

developed a process to stabilize the supraparticles by coating the surface by polyvinylpyrrolidone (PVP) and then by silica. The photoluminescence spectra of PVP- and silica-coated Si QDs supraparticles were very similar to those of Si QDs dispersed in solution.

INTRODUCTION

A mesoscale particle produced by clustering nanoparticles (NPs) via weak physical interactions is dubbed as a supraparticle[1, 2]. Formation of a supraparticle modifies the property of constituent NPs via coupling of the electronic wavefunctions, Förster resonant energy transfer (FRET), etc. Supraparticles have been produced from a variety of materials including metal[3], semiconductor[4-8] and organic[9-12] materials. In a supraparticle made from metal NPs, the coupling modifies the localized surface plasmon resonances[3], while that made from semiconductor quantum dots (QDs), FRET modifies the light emission property[4]. A supraparticle can be an optical cavity to confine photons, which results in the structural coloration[5]. In relatively large supraparticles, coupling of QD emission with the whispering gallery mode narrows the emission spectra[6, 8]. Furthermore, even if there are no NP-to-NP interactions, the structural feature that NPs are localized in a mesoscale space leads to useful properties. For example, the stronger light emission compared to individual QDs improves the detection limit of fluorescence bioimaging. The capability to mix different size QDs leads to wide range control of the emission color[7]. Furthermore, colocalization of magnetic NPs and semiconductor QDs results in magneto-fluorescent supraparticles, which are magnetically-manipulated and optically-tracked in living cells[13-15].

In this work, we develop supraparticles of silicon (Si) QDs. Si QDs are bio-compatible and biodegradable nanophosphors that have potential to take the place of cadmium and lead

chalcogenide QDs phosphors, especially in biomedical fields. Si QDs below 10 nm in diameter exhibit size-dependent luminescence in the red to near infrared (NIR) wavelength range due to the quantum size effects[16-19]. There have been numerous researches to use Si QDs phosphors for bio-imaging and -sensing[20-23]. Cytotoxicity of Si QDs to different human cells has been studied by fluorescence imaging[20, 21, 24, 25]. Furthermore, Si QDs can be conjugated with antibodies for bio-sensing using antigen-antibody reactions [23, 26].

A drawback to use isolated Si QDs as phosphors is the weak emission intensity due mainly to the small excitation (absorption) cross section and the small luminescence quantum yield. The problem can be partly solved by simply using agglomerates of Si QDs. The most widely used Si QDs agglomerates are porous Si NPs[27]. Very high contrast imaging has been achieved with porous Si NPs by using time-gated imaging [28, 29] and two-photon imaging[30] techniques. In time gated imaging, the long luminescence lifetime (> 10 μsec) of Si QDs is a great advantage to perfectly separate the fluorescence signal from the fast autofluorescence of bio-substances. Porous Si NPs are also promising for drag delivery because of the capability of incorporating molecules in the pores[31, 32]. Drawbacks of porous Si NPs are the large size and shape distributions and the relatively low luminescence quantum yield. Another approach to form Si QDs agglomerates is the micelle encapsulation[33]. In vivo targeted cancer imaging has been demonstrated by using micelle encapsulated Si QDs [33].

The purpose of this work is to develop red-to-NIR luminescent spherical supraparticles made from Si QDs by a controlled manner for the fluorescence bio-imaging applications. Among different methods to produce supraparticles[1], we employ a self-limited self-assembly process. The process has been extensively used for the preparation of supraparticles from colloidal solutions of NPs. In the self-limited self-assembly process, colloidally stable supraparticles are produced by

controlling the balance of the repulsive and attractive forces between NPs; reduction of repulsive forces initiate agglomeration of NPs and the self-assembly stops when the attractive and repulsive interactions reach an equilibrium state[1]. In supraparticles produced by this process, NPs are densely packed and often close-packed superlattice structures are spontaneously formed[34]. In this work, we employ a methanol solution of colloidally stable all-inorganic Si QDs developed in our group as a starting material [35]. In the Si QDs, boron (B) and phosphorus (P) are simultaneously doped (B and P codoped Si QDs) and the QD is composed of a crystalline Si core and a heavily B and P codoped amorphous shell[35, 36]. The amorphous shell induces negative potential on the surface and makes the QD dispersible in polar solvents such as methanol[37, 38] and water[39]. We show that by adding a small amount of toluene to the methanol solution of Si QDs, uniform size supraparticles are spontaneously formed. We also develop a process to stabilize the structure by silica coating. Finally, we discuss the photoluminescence (PL) property of Si QDs supraparticles.

RESULTS AND DISCUSSION

Figure 1(a) shows a picture of a methanol solution of B and P codoped Si QDs grown at 1200°C. The solution is very clear and light scattering by agglomerates is not observed. In fact, light transmittance below the band gap energy of bulk Si crystal is almost 100% (Figure 1(b)). Figure 1(c) shows the transmission electron microscope (TEM) image of Si QDs grown at 1200°C. For the TEM observation, the Si QD solution was dropped on a graphene-oxide-coated copper mesh and dried[36]. Si QDs are isolated on the support film and no three-dimensional agglomerates are observed. These results indicate that Si QDs are perfectly dispersed in methanol. The high dispersibility of codoped Si QDs in polar solvents is due to the negative surface potential (zeta potential: -40–-50 mV)[20, 39]. Note that the Si QDs are not dispersible in nonpolar solvents such as

toluene. The high-resolution TEM image in the inset reveals that the Si QD is composed of a crystalline core and an amorphous shell[36]. The lattice spacing corresponds to {111} planes of Si crystal. The amorphous shell is composed of B, Si and P, and the thickness can be controlled by growth parameters[36]. The average diameter estimated from TEM images is 7.1 nm with the standard deviation of 1.6 nm. Figure 1(d) shows the PL spectra of Si QDs in methanol excited at 405 nm. The luminescence appears in the red to NIR range and the high energy shift of the PL energy with decreasing the size is clearly observed [38, 40].

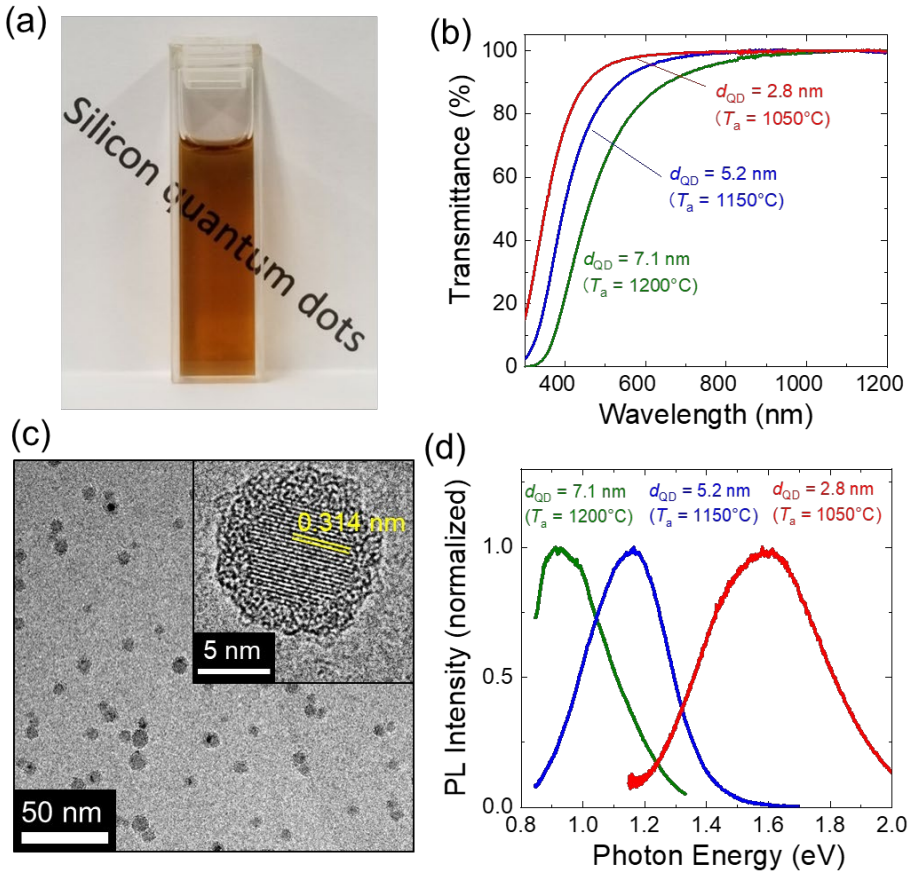

Figure 1. (a) Methanol solution of B and P codoped Si QDs grown at 1200°C. (b) Light transmittance spectra of Si QDs grown at different temperatures. The average diameter (d_{QD}) and the growth temperature (T_a) of Si QDs are shown in the figure. (c) TEM image of Si QDs grown

at 1200°C. Inset is the high-resolution TEM image of a Si QD. (d) PL spectra of Si QDs dispersed in methanol. The average diameter and the growth temperature of Si QDs are shown in the figure.

Scheme 1 shows the procedure to produce Si QDs supraparticles. First, a methanol solution of Si QDs is prepared in microtubes (1.5 mL) by the procedure shown in the EXPERIMENTAL METHODS section[35]. Toluene is then added to the solution as a poor solvent and the microtube is gently shaken to promote agglomeration of Si QDs. This process changes the solution from transparent to cloudy as can be seen in the photos in Scheme 1. All the processes are performed in usual laboratory atmosphere at room temperature. The number density of Si QDs in the solutions (N_{QD}) is changed from 1.2×10^{15} to 1.7×10^{17} cm^{-3}, while the amount of toluene in the mixed solutions (C_{PhMe}) is changed from 66.7 to 97.6 vol.%. Si QDs with the average diameter (d_{QD}) of 2.8, 5.2 and 7.1 nm are used for the preparation of supraparticles.

Scheme 1. Preparation procedure Si QDs supraparticles.

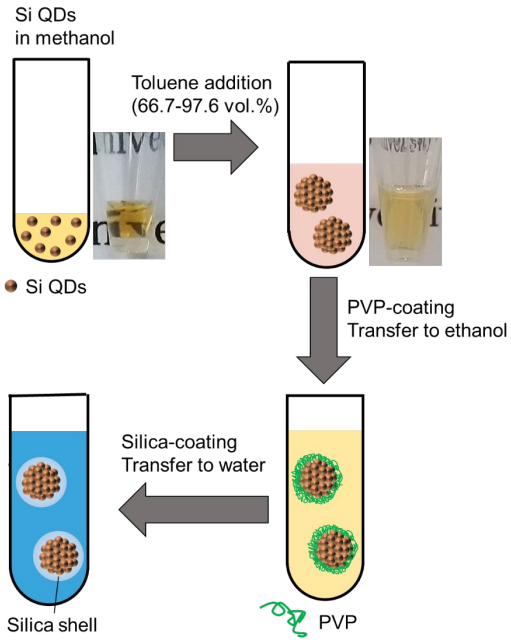

Figure 2(a) shows a TEM image of supraparticles. The enlarged image is shown in Figure 2(b). The average diameter and the density of Si QDs used for the preparation of the supraparticles are 2.8 nm and 5.5×10^{16} cm^{-3}, respectively. The toluene concentration is 75.0 vol.%. We can see the formation of spherical supraparticles simply by adding toluene to a methanol solution of Si QDs. Figure 2(c) shows a supraparticle produced from Si QDs 5.2 nm in average diameter (N_{QD}=2.1×10^{16} cm^{-3}, C_{PhMe}=88.9%). Individual Si QDs constituting the supraparticle can be recognized. In the Supporting Information (Figure S1), we show TEM images of supraparticles produced with different parameters. In the images in Figure S1, individual Si QDs composing a supraparticle are visible. Figure 2(d) shows a peripheral region of a supraparticle produced from Si QDs 7.1 nm in average diameter (N_{QD}=3.5×10^{15} cm^{-3}, C_{PhMe}=83.3%). The lattice fringes correspond to {111} planes of Si crystal. We can see that Si QDs are densely packed in the supraparticle. This is due to the ligand-free surface of the Si QDs used for the formation of the supraparticles. Figure 2(e) shows the fast Fourier transform (FFT) image of the region surrounded

by a square in Figure 2(d). Diffraction spots corresponding to {111} planes of Si crystal can clearly be seen. Figure 2(f) shows a scanning electron microscope (SEM) images of a Si QDs supraparticle (d_{QD}=2.8 nm, N_{QDs}=1.7×10^{17} cm^{-3}, C_{PhMe}=75%) placed on a Si wafer observed without tilting and with the tilting angle of 25°. Without tilting, the aspect ratio is 1.0, while it is about 0.88 under 25° tilting. Therefore, the supraparticle is only slightly squashed when it is dried on a substrate.

Si QDs supraparticles similar to those in Figure 2(a)-(f) are formed in specific parameter ranges. Figure 2(g) summarizes the experimental conditions for the formation of supraparticles. The abscissa is the toluene concentration and the ordinate is the number density of Si QDs. TEM images of particles produced by 8 different conditions in Figure 2(g) are summarized in the Supporting Information (Figure S2). The red, blue and green colors correspond to Si QDs 2.8, 5.2 and 7.1 nm in average diameters, respectively. In the conditions shown by the circles, spherical supraparticles are formed, while those shown by squares, linear chains of supraparticles are formed. In the conditions designated by ×, random networks of Si QDs are formed (see Figure S2(g) in the Supporting Information, while those designated by +, agglomerates are precipitated. In the condition designated by a triangle, spherical supraparticles and random networks of Si QDs are mixed. We can see that isolated supraparticles are formed predominantly in a specific region marked by a yellow dotted curve although there are several exceptions. Outside the region, supraparticles are not formed; in the lower left and the left of the region, agglomeration does not proceed promptly, while in the upper right and the right of the region, large agglomerates precipitate. The optimum range for the formation of supraparticles does not seem to depend strongly on the size of Si QDs in the diameter range from 2.8 nm to 7.1 nm. However, there seems to be a slight tendency that higher QD density and higher toluene concentration are necessary for the growth of supraparticles from smaller QDs.

Within the optimum ranges of supraparticle formation conditions, the size tends to increase with increasing toluene concentration. Figure 2(h) shows the size distribution of supraparticles estimated from the TEM images. The size and the concentration of Si QDs are fixed to 2.8 nm and 3.6×10^{16} cm^{-3}, respectively, while only the toluene concentration is changed from 80.0% to 87.5%. With increasing the toluene concentration, the average diameter of supraparticles (d_{Sup}) increases from 101 nm to 159 nm (Figure S3 in the Supporting Information). The full width at half maximum (FWHM) of the size distribution is around 50% of the average diameter.

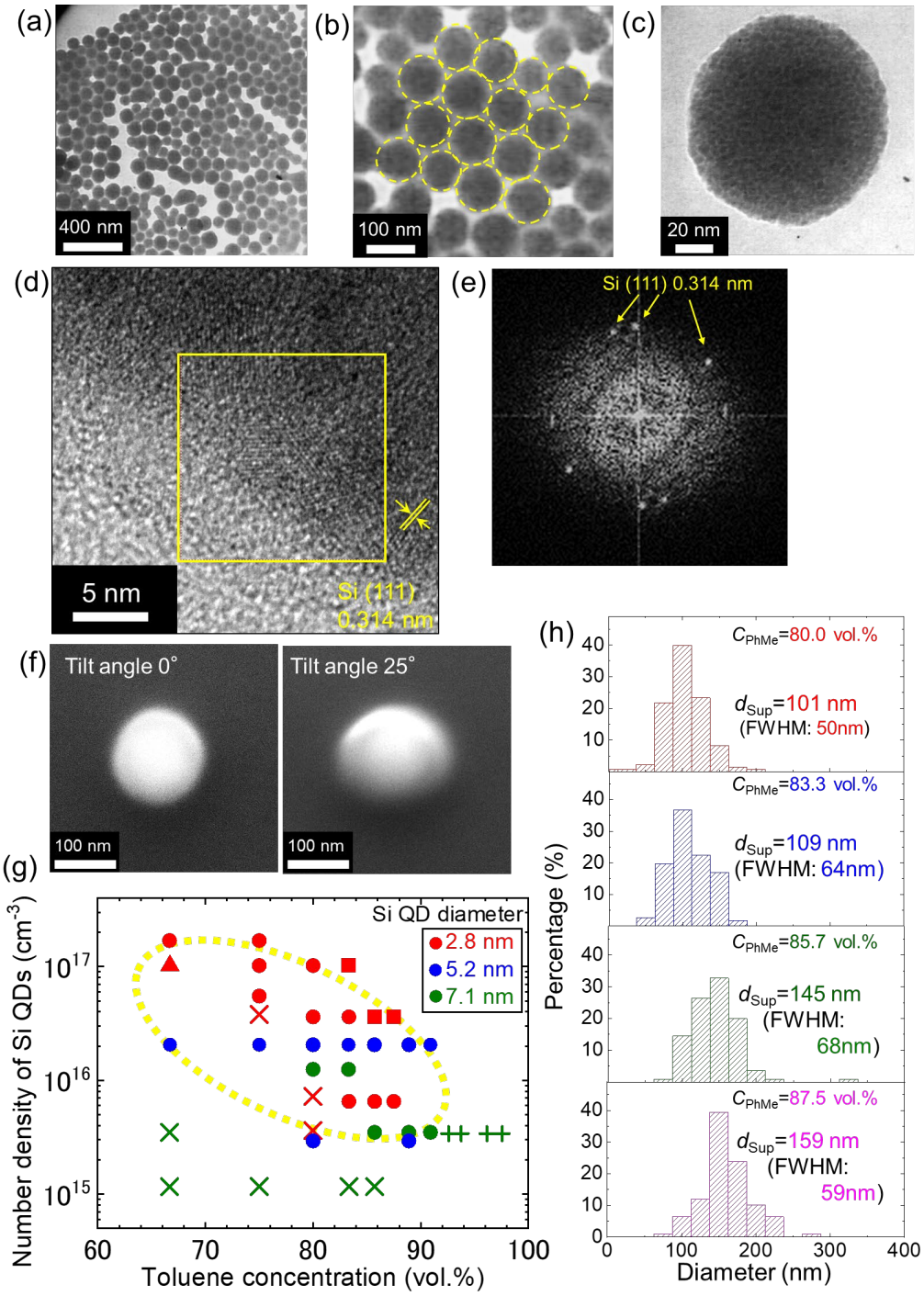

Figure 2. (a) TEM image of Si QDs supraparticles (d_{QD}=2.8 nm, N_{QD}=5.5×10^{16} cm^{-3}, C_{PhMe}=75.0%). (b) Enlarged image of (a). (c) TEM image of a supraparticle (d_{QD}=5.2 nm, N_{QD}=2.1×10^{16} cm^{-3}, C_{PhMe}=88.9%). (d) TEM image of a peripheral region of a supraparticle

(d_{QD}=7.1 nm, N_{QD}=3.5×10^{15} cm^{-3}, C_{PhMe}=83.3%). (e) FFT image of the region surrounded by a square in (d). (f) SEM images of a supraparticle taken without tilting and under 25° tilting (d_{QD}=2.8 nm, N_{QD}=1.7×10^{17} cm^{-3}, C_{PhMe}=75%). (g) Conditions for the formation of supraparticles. Red, blue and green colors correspond to Si QDs 2.8, 5.2 and 7.1 nm in average diameters, respectively. Circles represent formation of isolated spherical supraparticles, while squares represent formation of linear chains of supraparticles. × represents growth of indeterminate shape agglomerates, and + represents precipitation of large agglomerates. Δ represents mixture of spherical supraparticles and indeterminate shape agglomerates. (h) Size distribution of supraparticles. d_{QD} and N_{QD} are fixed to 2.8 nm and 3.6×10^{16} cm^{-3}, respectively, and C_{PhMe} is changed from 80 to 87.5%.

The data in Figure 2 are obtained just after preparation of supraparticles, *i.e.*, a solution of Si QDs supraparticles are dropped on a TEM mesh or on a Si wafer just after preparation. If we keep supraparticles in methanol/toluene mixed solutions longer, secondary agglomeration slowly proceeds. This can be seen in the TEM images in the Supporting Information (Figure S4(a)). Already after 1 h from the preparation, linear chains of supraparticles are formed and after 2 h, three-dimensional agglomerates are formed. We tried several different processes to stop secondary agglomeration of supraparticles in solutions. The most successful process was simply adding a large amount of methanol just after the formation of supraparticles. In the Supporting Information (Figure S4(b)), TEM images of supraparticles stabilized by this process are shown. 500 μL of methanol was added to an 80 μL methanol/toluene solution of Si QDs supraparticles (d=2.8 nm, N_{QDs}=1.7×10^{17} cm^{-3}, C_{PhMe}=75%), i.e., C_{PhMe} is reduced from 75% to 10.3% by adding methanol. With this procedure, agglomeration of supraparticles is perfectly prevented; even after 2 months from the preparation, no agglomerates are observed (Figure S4(b) in the Supporting Information).

Therefore, addition of methanol effectively stops secondary agglomeration of supraparticles. Interestingly, the methanol addition does not affect the shape of individual supraparticles, i.e., supraparticles are not decomposed into individual QDs in the methanol-rich solution. At present, the mechanism of this irreversibility, i.e., the supraparticles are structurally stable in methanol-rich solution, is not very clear. Probably, the fact that Si QDs are directly attached each other in a supraparticle because of the ligand-free surface is responsible for the high structural stability.

For many applications of supraparticles, especially for the biomedical applications, the capability to be functionalized with a variety of molecules is indispensable. To this end, supraparticles are often coated by a silica layer[14, 41]. Therefore, we develop a process to coat Si QDs supraparticles by a thin silica layer. The silica-coating process is composed of two steps (Scheme 1). After preparation of supraparticles, we first cover the surface by polyvinylpyrrolidone (PVP) by the process shown in the EXPERIMENTAL MTHODS section and disperse them in ethanol. Figure 3(a) and (b) shows SEM and TEM images of PVP coated supraparticles (d_{QDs}=2.8 nm, N_{QDs}=1.7×10^{17} cm^{-3}, C_{PhMe}=75%). PVP coating stabilizes the structure of supraparticles and the structure is kept for more than one week. Other TEM images of PVP-coated supraparticles are shown in the Supporting Information (Figure S5). On the surface of PVP-coated supraparticles in ethanol, a thin silica layer can be grown by the Stöber method [42-45]. Figure 3(c) shows a TEM image of silica-coated supraparticles and Figure 3(d) is an enlarged image. We can see that the surface is covered by a layer of silica NPs and not very smooth. The thickness of the silica nanoparticle layer is about 5-10 nm. Other TEM images of silica-coated supraparticles are shown in the Supporting Information (Figure S6). Figure 3(e) shows number distributions of PVP-coated and silica-coated Si QDs supraparticles measured by dynamic light scattering (DLS) (Otsuka, nanoSAQLA). The average diameter decreases from 149 nm to 127 nm after the silica shell growth.

This suggests that PVP bulky polymer layers are removed during the silica coating process [14]. The TEM and DLS data demonstrate that no significant agglomeration occurs during the coating process and the supraparticles are colloidally stable in water. The silica-coated supraparticles are stable in water for more than 5 months (see DLS data after 5 months from the preparation in the Supporting Information (Figure S7)).

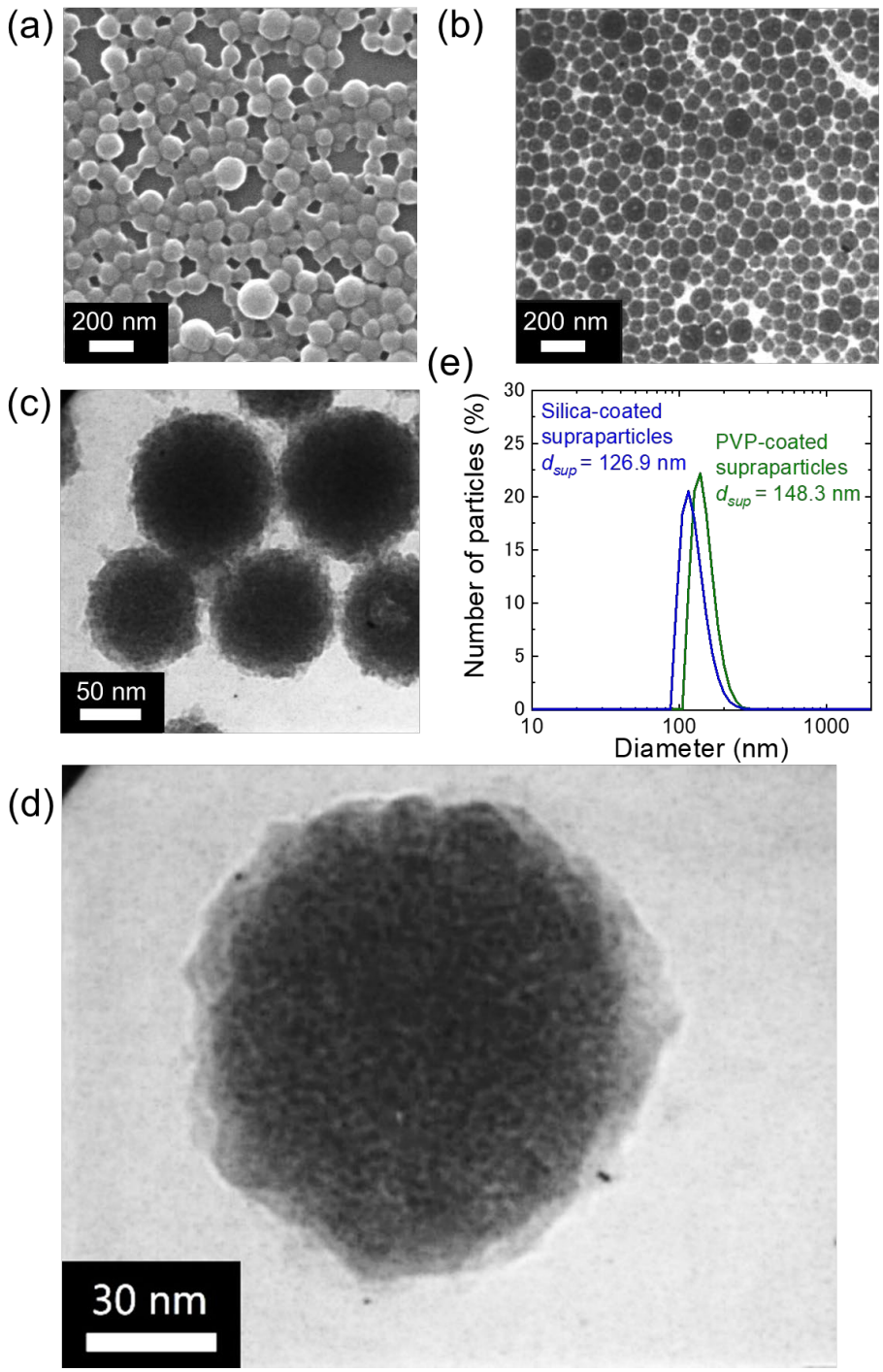

Figure 3. (a) SEM image of PVP-coated Si QDs supraparticles. (b) TEM image of PVP-coated Si QDs supraparticles. (c, d) TEM images of silica-coated Si QDs supraparticles. (e) Number distributions of PVP-coated and silica-coated Si QDs supraparticles.

Finally, we study the PL properties of supraparticles. Figure 4(a) shows the normalized PL spectra of Si QDs dispersed in methanol, PVP-coated supraparticles and silica-coated supraparticles produced from the same Si QDs solution. We can see that the PL spectrum is not strongly modified by the formation of supraparticles and PVP- and silica-coating. Figure 4(b) shows the PL decay curves detected at 1.57 eV. The decay curves are not a single-exponential function. The non-exponential decay curve has been commonly observed for many kinds of Si nanocrystal systems, and the decay curves are often fitted by the stretched exponential function, $I = I_0 \exp\left[-(t/\tau)^{\beta}\right]$, where τ is the apparent decay constant and β is the stretching parameter[46]. Figure 4(c) shows the decay rates $(1/\tau)$ at different detection energies. The decay rate is significantly enhanced by the formation of supraparticles. In the Supporting Information (Figure S8), we also show the decay curve and decay rates of supraparticles before PVP-coating. The decay rate enhancement is the most significant at the step of the supraparticle formation, and after that, the decay rate increases slightly by PVP-coating and silica-coating. This suggests that agglomeration of Si QDs is a major cause of the decay rate enhancement[47-49].

There are several possible mechanisms of the agglomeration-induced enhancement of the PL decay rate. In the present supraparticle formation process, the decay rate enhancement due to surface modification of individual Si QDs is unlikely considering the very mild preparation process. Another possible mechanism of the decay rate enhancement is the different local photonic mode density (Purcell factor) between Si QDs in methanol and supraparticles due to the different dielectric environment of individual Si QDs. In a previous work, we studied the effect of the dielectric environment on the decay rate of Si QDs in detail and found that the effect is not negligible if we compare the decay rates of Si QDs in methanol and those in Si QDs solids[49]. This

is due to the large difference in the dielectric permittivity between methanol and Si QDs solids; the permittivity of methanol is 1.77, while that of Si QDs solids reaches ~6 if Si QDs are closely packed[49]. Although we cannot quantitatively estimate the contribution of the Purcell effect on the decay rate enhancement, it is possible that the decay rate enhancement in Figure 4(c), especially at the low detection energy range, where larger Si QDs in the size distribution contribute to the PL, is partly due to the Purcell enhancement. In our previous work, the most important effect affecting the decay rate enhancement in Si QDs solids was the energy transfer between Si QDs[47-49]. Since the energy transfer occurs from smaller Si QDs having larger band gap to larger Si QDs having smaller band gap in the size distribution, the decay rate enhancement becomes larger at the higher PL detection energy. This is consistent with the data in Figure 4(c). Furthermore, quenching of PL from smaller Si QDs by the energy transfer results in apparent low-energy shift of inhomogeneously broadened PL spectra. This is also observed in Figure 4(a). Therefore, the energy transfer is considered to be the major mechanism of the observed decay rate enhancement by the formation of supraparticles.

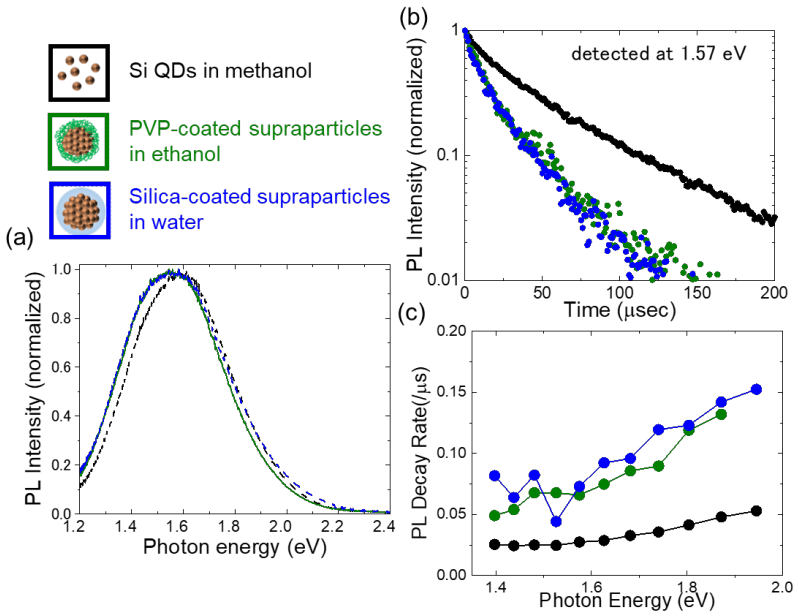

Figure 4. (a) PL spectra of Si QDs dispersed in methanol, PVP-coated Si QDs supraparticles in ethanol and silica-coated Si QDs supraparticles in water. (b) PL decay curves detected at 1.57 eV. (c) PL decay rate as a function of detection energy.

It is not straightforward to compare the luminescence intensity of supraparticles with that of Si QDs dispersed in solution due to the significantly different light scattering properties; there is no light scattering in a Si QDs-dispersed solution, while significant light scattering is observed in a supraparticles-dispersed solution. We used the method explained in detail in the EXPERIMENTAL METHOD to compare relative PL quantum yields (QYs) between Si QDs dispersed in solution and supraparticles. We found that the QY decreases to 36% of that of Si QDs dispersed in methanol in PVP-coated supraparticles, and it decreases to 18% in silica-coated supraparticles. Since the PL QY of the Si QDs dispersed in methanol is 12.8%, those of PVP-coated and silica-coated supraparticles are 4.6% and 2.3%, respectively. The decrease of the QYs by the formation of supraparticles indicates that the observed shortening of the PL lifetime is

mainly due to the energy transfer between Si QDs in a supraparticle; energy transfer between Si QDs increases the chance that excitons migrate to non-luminescing "dark" Si QDs and recombine nonradiatively. Reducing the size distribution may be useful to prevent the energy transfer, because it occurs from smaller to larger Si QDs[48, 49]. Coating the surface of individual Si QDs by silica may also be effective to prevent the exciton migration, because the efficiency of FRET depends strongly on NP-to-NP distances[48, 49]. Although the luminescence QYs of supraparticles are lower than that of individual Si QDs at the present stage of research, considering the number of Si QDs forming a supraparticle, the luminescence intensity itself is much larger. In a close-packed structure, a 100 nm supraparticle is composed of more than 10,000 2.8 nm diameter QDs. This is an advantage for applications that do not require single nm size QDs and is suitable for ~100 nm size particles.

CONCLUSION

We have succeeded in producing red-to-NIR luminescent supraparticles of Si QDs by a facile self-limited self-assembly process. We demonstrated that simply by adding toluene to a methanol solution of Si QDs, spherical supraparticles around 100 nm in diameters with narrow size distributions are spontaneously formed. We also developed a process to stabilize the supraparticles by coating the surface by PVP and then by silica. The PL spectra of PVP- and silica-coated Si QDs supraparticles were very similar to those of Si QDs dispersed in methanol. We believe that the development of the process to produce spherical agglomerates of Si QDs by a controlled manner promotes the application as phosphors especially in biomedical fields.

EXPERIMENTAL METHODS

Preparation of B and P codoped Si QDs

Si QDs with B and P codoped shells (B and P codoped Si QDs) were prepared by the procedure described in detail in our previous papers[35]. Briefly, thick Si-rich borophosphosilicate glass (BPSG) films were deposited on a stainless-steel plate by simultaneously sputtering Si, SiO_2, B_2O_3, and phosphosilicate glass (PSG) (SiO_2:P_2O_5=95:5 wt.%). The B and P concentrations in Si-rich BPSG were 0.9 atom% and 0.6 atom%, respectively. The Si-rich BPSG films were then peeled off from the stainless-steel plate and annealed in a N_2 gas atmosphere at 1050, 1150 and 1200°C for 30 min to grow B and P codoped Si QDs in a BPSG matrix. The average diameters of Si QDs grown at 1050, 1150 and 1200°C were 2.8, 5.2 and 7.1 nm, respectively. Finally, Si QDs were extracted from the matrix by hydrofluoric acid (HF) etching, and then transferred to methanol and stored for more than 7 days. During the storage, very thin native oxides are formed on the surface of Si QDs.

Silica coating

Supraparticles were first coated by amphiphilic PVP and then by silica by the Stöber method[43] The procedure of the PVP coating is as follows. PVP K30 (Wako) was dissolved in a 25:75 mixture solution of methanol and toluene to produce a PVP solution (5 mg/mL). 20 μL of the PVP solution was added to a 80 μL methanol/toluene mixture solution of Si QDs (d=2.8 nm, N_{QDs}=1.7×10^{17} cm^{-3}, C_{PhMe}=75%) and sonicated for 20 min. After repeating the processes for three times, the solution was centrifuged (7000-10000 rpm, 4680-9560 G) to separate PVP-coated supraparticles from the solution. Ethanol (Wako, 99.5%) was then added to redisperse supraparticles in ethanol.

On the surface of PVP-coated supraparticles, silica shell was formed by the Stöber method [42-45]. Typical experimental parameters are as follows. Tetraethoxysilane (TEOS) (Wako, 95.0%) was diluted by ethanol to 0.3 vol.%. 20 μL of the TEOS solution was added to 200 μL ethanol solution of PVP-coated supraparticles. After ultrasonication for 5 min, 20 μL ultrapure water and 20 μL

ammonia solution (Wako, 28.0%) were added and ultrasonicated for 1 h. The solution was centrifuged (7000-10000 rpm, 4680-9560 G) to separate silica-coated supraparticles. Ultrapure water was then added to redisperse supraparticles in water.

Characterization of supraparticles

TEM observations were performed by JEM-2100F (JEOL) operated at 200 kV and H-7000 (Hitachi) operated at 100 kV. For the TEM observations of Si QDs and Si QDs supraparticles, the solutions were dropped on a graphene-oxide-coated copper mesh and dried. For the measurements of the size distributions of supraparticles, diameters (d) of more than 100 particles were measured on imageJ software, and the histograms were fitted by a log-normal distribution function, $f(d) = \frac{1}{\sqrt{2\pi}\sigma d}\exp\left(-\frac{(\ln d-\mu)^2}{2\sigma^2}\right)$, where σ and μ are fitting parameters. The mean value (d_{sup}) was calculated from the $d_{sup} = \exp(\mu + \frac{\sigma^2}{2})$ relation.

SEM observations were performed using JSM-7100F (JEOL). For the SEM observations of Si QDs supraparticles, the particles were placed on a Si wafer. The stage was tilted up to 25° to study the shape.

DLS measurements were performed using nanoSAQLA (Otsuka Electronics) at 25°C.

PL spectra and PL decay dynamics

PL spectra of Si QDs and Si QDs supraparticles were measured using a single spectrometer equipped with a liquid-N_2 cooled InGaAs diode array (OMA-V-SE, Roper Scientific) and a charge coupled device (CCD) (Roper Scientific). The excitation wavelength was 405 nm. Time-resolved PL spectra were excited by modulated 405 nm light and measured using a gated CCD (ICCD) (PI-MAX, Princeton Instruments).

Estimation of relative QYs

In order to estimate relative PL QYs of supraparticles with respect to that of Si QDs dispersed in solution, we first measured the PL spectra of the very diluted solutions by the setup shown in the Supporting Information (Figure S9(a)). The purpose of using very diluted solutions is to avoid scattering of excitation and emitted light by supraparticles. Furthermore, as can be seen in the Figure S9(a) in the Supporting Information, we collected the emission light from the region very close to the front surface of the 1cm×cm cuvette and very close to the entrance window of the excitation light to further avoid the scattering effect.

We then estimated the ratio of photons absorbed by Si QDs (absorptance) during the PL excitation process. In order to estimate the absorptance (A), we measured the diffuse reflectance (R) and diffuse transmittance (T) by using an integrating sphere by the setups shown in the Supporting Information (Figure S9(b) and (c), respectively) (SolidSpec 3700, Shimadzu). For these measurements, a thin quartz cuvette (2 mm light pass) was used. Finally, the absorptance is obtained from the A=1-R-T relation. By using the absorptance values at the PL excitation wavelength (405 nm), the PL spectra are normalized by the number of absorbed photons by Si QDs. Comparing the integral intensities of normalized PL spectra between Si QDs dispersed in solution and supraparticles in solution, the relative PL QYs of supraparticles are obtained.

ASSOCIATED CONTENT

Supporting Information.

The Supporting Information is available free of charge on the ACS Publications website at DOI:

Additional TEM images of Si QDs supraparticles, the relation between the mean diameter of supraparticles and the toluene concentration, DLS data of silica-coated Si QDs supraparticles

after 5 months from the preparation, PL decay curves and the decay rates of Si QDs supraparticles before coating, setups for PL, diffuse reflectance and diffuse transmittance measurements (PDF).

AUTHOR INFORMATION

Corresponding Author

*E-mail: fujii@eedept.kobe-u.ac.jp.

**E-mail: sugimoto@eedept.kobe-u.ac.jp

ORCID

Minoru Fujii: 0000-0003-4869-7399

Hiroshi Sugimoto: 0000-0002-1520-0940

Funding Sources

This work was partly supported by JSPS KAKENHI grant numbers 16H03828, 18K14092, 18KK0141 and 19K22111, and JSPS 2018 Bilateral Joint Research Projects (Japan−Australia).

Notes

The authors declare no competing financial interest.

REFERENCES

1. Wintzheimer, S.; Granath, T.; Oppmann, M.; Kister, T.; Thai, T.; Kraus, T.; Vogel, N.; Mandel, K., Supraparticles: Functionality from Uniform Structural Motifs. *ACS nano* **2018,** *12* (6), 5093-5120.

2. Piccinini, E.; Pallarola, D.; Battaglini, F.; Azzaroni, O., Self-limited self-assembly of nanoparticles into supraparticles: towards supramolecular colloidal materials by design. *Molecular Systems Design & Engineering* **2016,** *1* (2), 155-162.
3. Pazos-Perez, N.; Wagner, C. S.; Romo-Herrera, J. M.; Liz-Marzán, L. M.; García de Abajo, F. J.; Wittemann, A.; Fery, A.; Alvarez-Puebla, R. A., Organized Plasmonic Clusters with High Coordination Number and Extraordinary Enhancement in Surface-Enhanced Raman Scattering (SERS). *Angew. Chem. Int. Ed.* **2012,** *51* (51), 12688-12693.
4. Mayilo, S.; Hilhorst, J.; Susha, A. S.; Höhl, C.; Franzl, T.; Klar, T. A.; Rogach, A. L.; Feldmann, J., Energy Transfer in Solution-Based Clusters of CdTe Nanocrystals Electrostatically Bound by Calcium Ions. *J. Phys. Chem. C* **2008,** *112* (37), 14589-14594.
5. Park, J.-G.; Kim, S.-H.; Magkiriadou, S.; Choi, T. M.; Kim, Y.-S.; Manoharan, V. N., Full-Spectrum Photonic Pigments with Non-iridescent Structural Colors through Colloidal Assembly. *Angew. Chem. Int. Ed.* **2014,** *53* (11), 2899-2903.
6. Vanmaekelbergh, D.; van Vugt, L. K.; Bakker, H. E.; Rabouw, F. T.; de Nijs, B.; van Dijk-Moes, R. J. A.; van Huis, M. A.; Baesjou, P. J.; van Blaaderen, A., Shape-Dependent Multiexciton Emission and Whispering Gallery Modes in Supraparticles of CdSe/Multishell Quantum Dots. *ACS nano* **2015,** *9* (4), 3942-3950.
7. Montanarella, F.; Altantzis, T.; Zanaga, D.; Rabouw, F. T.; Bals, S.; Baesjou, P.; Vanmaekelbergh, D.; van Blaaderen, A., Composite Supraparticles with Tunable Light Emission. *ACS nano* **2017,** *11* (9), 9136-9142.
8. Montanarella, F.; Urbonas, D.; Chadwick, L.; Moerman, P. G.; Baesjou, P. J.; Mahrt, R. F.; van Blaaderen, A.; Stöferle, T.; Vanmaekelbergh, D., Lasing Supraparticles Self-Assembled from Nanocrystals. *ACS nano* **2018,** *12* (12), 12788-12794.
9. Liljeström, V.; Seitsonen, J.; Kostiainen, M. A., Electrostatic Self-Assembly of Soft Matter Nanoparticle Cocrystals with Tunable Lattice Parameters. *ACS nano* **2015,** *9* (11), 11278-11285.
10. Moerz, S. T.; Kraegeloh, A.; Chanana, M.; Kraus, T., Formation Mechanism for Stable Hybrid Clusters of Proteins and Nanoparticles. *ACS nano* **2015,** *9* (7), 6696-6705.
11. Piccinini, E.; Pallarola, D.; Battaglini, F.; Azzaroni, O., Recognition-driven assembly of self-limiting supramolecular protein nanoparticles displaying enzymatic activity. *Chem. Commun.* **2015,** *51* (79), 14754-14757.
12. Picco, A. S.; Yameen, B.; Knoll, W.; Ceolín, M. R.; Azzaroni, O., Temperature-driven self-assembly of self-limiting uniform supraparticles from non-uniform unimolecular micelles. *J. Colloid Interface Sci.* **2016,** *471*, 71-75.
13. Yang, G.; Zhong, H.; Liu, R.; Li, Y.; Zou, B., In Situ Aggregation of ZnSe Nanoparticles into Supraparticles: Shape Control and Doping Effects. *Langmuir* **2013,** *29* (6), 1970-1976.
14. Chen, O.; Riedemann, L.; Etoc, F.; Herrmann, H.; Coppey, M.; Barch, M.; Farrar, C. T.; Zhao, J.; Bruns, O. T.; Wei, H.; Guo, P.; Cui, J.; Jensen, R.; Chen, Y.; Harris, D. K.; Cordero, J. M.; Wang, Z.; Jasanoff, A.; Fukumura, D.; Reimer, R.; Dahan, M.; Jain, R. K.; Bawendi, M. G., Magneto-fluorescent core-shell supernanoparticles. *Nature Commun.* **2014,** *5* (1), 5093.
15. Yang, F.; Skripka, A.; Tabatabaei, M. S.; Hong, S. H.; Ren, F.; Benayas, A.; Oh, J. K.; Martel, S.; Liu, X.; Vetrone, F.; Ma, D., Multifunctional Self-Assembled Supernanoparticles for Deep-Tissue Bimodal Imaging and Amplified Dual-Mode Heating Treatment. *ACS nano* **2019,** *13* (1), 408-420.

16. Yu, Y.; Fan, G.; Fermi, A.; Mazzaro, R.; Morandi, V.; Ceroni, P.; Smilgies, D.-M.; Korgel, B. A., Size-Dependent Photoluminescence Efficiency of Silicon Nanocrystal Quantum Dots. *J. Phys. Chem. C* **2017,** *121* (41), 23240-23248.
17. Pringle, T. A.; Hunter, K. I.; Brumberg, A.; Anderson, K. J.; Fagan, J. A.; Thomas, S. A.; Petersen, R. J.; Sefannaser, M.; Han, Y.; Brown, S. L.; Kilin, D. S.; Schaller, R. D.; Kortshagen, U. R.; Boudjouk, P. R.; Hobbie, E. K., Bright Silicon Nanocrystals from a Liquid Precursor: Quasi-Direct Recombination with High Quantum Yield. *ACS nano* **2020,** *14* (4), 3858-3867.
18. Mastronardi, M. L.; Maier-Flaig, F.; Faulkner, D.; Henderson, E. J.; Kubel, C.; Lemmer, U.; Ozin, G. A., Size-dependent absolute quantum yields for size-separated colloidally-stable silicon nanocrystals. *Nano Lett.* **2012,** *12* (1), 337-42.
19. Sangghaleh, F.; Sychugov, I.; Yang, Z.; Veinot, J. G. C.; Linnros, J., Near-Unity Internal Quantum Efficiency of Luminescent Silicon Nanocrystals with Ligand Passivation. *ACS nano* **2015,** *9* (7), 7097-7104.
20. Ostrovska, L.; Broz, A.; Fucikova, A.; Belinova, T.; Sugimoto, H.; Kanno, T.; Fujii, M.; Valenta, J.; Kalbacova, M. H., The impact of doped silicon quantum dots on human osteoblasts. *Rsc Advances* **2016,** *6* (68), 63403-63413.
21. Belinova, T.; Vrabcova, L.; Machova, I.; Fucikova, A.; Valenta, J.; Sugimoto, H.; Fujii, M.; Hubalek Kalbacova, M., Silicon Quantum Dots and Their Impact on Different Human Cells. *physica status solidi (b)* **2018,** *255* (10), 1700597.
22. Sakiyama, M.; Sugimoto, H.; Fujii, M., Long-lived luminescence of colloidal silicon quantum dots for time-gated fluorescence imaging in the second near infrared window in biological tissue. *Nanoscale* **2018,** *10* (29), 13902-13907.
23. Yanagawa, H.; Inoue, A.; Sugimoto, H.; Shioi, M.; Fujii, M., Antibody-conjugated near-infrared luminescent silicon quantum dots for biosensing. *MRS Communications* **2019,** *9* (3), 1079-1086.
24. Zhi, B.; Mishra, S.; Hudson-Smith, N. V.; Kortshagen, U. R.; Haynes, C. L., Toxicity Evaluation of Boron- and Phosphorous- Doped Silicon Nanocrystals towards Shewanella oneidensis MR-1. *ACS Applied Nano Materials* **2018,** *1* (9), 4884-4893.
25. Pramanik, S.; Hill, S. K. E.; Zhi, B.; Hudson-Smith, N. V.; Wu, J. J.; White, J. N.; McIntire, E. A.; Kondeti, V. S. S. K.; Lee, A. L.; Bruggeman, P. J.; Kortshagen, U. R.; Haynes, C. L., Comparative toxicity assessment of novel Si quantum dots and their traditional Cd-based counterparts using bacteria models Shewanella oneidensis and Bacillus subtilis. *Environmental Science: Nano* **2018,** *5* (8), 1890-1901.
26. Robidillo, C. J. T.; Aghajamali, M.; Faramus, A.; Sinelnikov, R.; Veinot, J. G. C., Interfacing enzymes with silicon nanocrystals through the thiol–ene reaction. *Nanoscale* **2018,** *10* (39), 18706-18719.
27. Park, J.-H.; Gu, L.; von Maltzahn, G.; Ruoslahti, E.; Bhatia, S. N.; Sailor, M. J., Biodegradable luminescent porous silicon nanoparticles for in vivo applications. *Nat Mater* **2009,** *8* (4), 331-336.
28. Gu, L.; Hall, D. J.; Qin, Z.; Anglin, E.; Joo, J.; Mooney, D. J.; Howell, S. B.; Sailor, M. J., In vivo time-gated fluorescence imaging with biodegradable luminescent porous silicon nanoparticles. *Nature Commun.* **2013,** *4*, 2326.
29. Joo, J.; Liu, X.; Kotamraju, V. R.; Ruoslahti, E.; Nam, Y.; Sailor, M. J., Gated Luminescence Imaging of Silicon Nanoparticles. *ACS nano* **2015,** *9* (6), 6233-6241.

30. Kim, D.; Kang, J.; Wang, T.; Ryu, H. G.; Zuidema, J. M.; Joo, J.; Kim, M.; Huh, Y.; Jung, J.; Ahn, K. H.; Kim, K. H.; Sailor, M. J., Two-Photon In Vivo Imaging with Porous Silicon Nanoparticles. *Adv. Mater.* **2017,** *29* (39), 1703309.
31. Kwon, E. J.; Skalak, M.; Bertucci, A.; Braun, G.; Ricci, F.; Ruoslahti, E.; Sailor, M. J.; Bhatia, S. N., Porous Silicon Nanoparticle Delivery of Tandem Peptide Anti-Infectives for the Treatment of Pseudomonas aeruginosa Lung Infections. *Adv. Mater.* **2017,** *29* (35), 1701527.
32. Li, W.; Liu, Z.; Fontana, F.; Ding, Y.; Liu, D.; Hirvonen, J. T.; Santos, H. A., Tailoring Porous Silicon for Biomedical Applications: From Drug Delivery to Cancer Immunotherapy. *Adv. Mater.* **2018,** *30* (24), 1703740.
33. Erogbogbo, F.; Yong, K. T.; Roy, I.; Hu, R.; Law, W. C.; Zhao, W.; Ding, H.; Wu, F.; Kumar, R.; Swihart, M. T.; Prasad, P. N., In vivo targeted cancer imaging, sentinel lymph node mapping and multi-channel imaging with biocompatible silicon nanocrystals. *ACS nano* **2011,** *5* (1), 413-23.
34. Zhuang, J.; Wu, H.; Yang, Y.; Cao, Y. C., Supercrystalline Colloidal Particles from Artificial Atoms. *Journal of the American Chemical Society* **2007,** *129* (46), 14166-14167.
35. Fujii, M.; Sugimoto, H.; Imakita, K., All-inorganic colloidal silicon nanocrystals-surface modification by boron and phosphorus co-doping. *Nanotechnology* **2016,** *27* (26), 262001.
36. Sugimoto, H.; Yamamura, M.; Sakiyama, M.; Fujii, M., Visualizing a core-shell structure of heavily doped silicon quantum dots by electron microscopy using an atomically thin support film. *Nanoscale* **2018,** *10* (16), 7357-7362.
37. Sugimoto, H.; Fujii, M.; Imakita, K.; Hayashi, S.; Akamatsu, K., Phosphorus and Boron Codoped Colloidal Silicon Nanocrystals with Inorganic Atomic Ligands. *J. Phys. Chem. C* **2013,** *117* (13), 6807-6813.
38. Sugimoto, H.; Fujii, M.; Imakita, K.; Hayashi, S.; Akamatsu, K., Codoping n- and p-Type Impurities in Colloidal Silicon Nanocrystals: Controlling Luminescence Energy from below Bulk Band Gap to Visible Range. *J. Phys. Chem. C* **2013,** *117* (22), 11850-11857.
39. Sugimoto, H.; Fujii, M.; Fukuda, Y.; Imakita, K.; Akamatsu, K., All-inorganic water-dispersible silicon quantum dots: highly efficient near-infrared luminescence in a wide pH range. *Nanoscale* **2014,** *6* (1), 122-126.
40. Sugimoto, H.; Yamamura, M.; Fujii, R.; Fujii, M., Donor-Acceptor Pair Recombination in Size-Purified Silicon Quantum Dots. *Nano Lett.* **2018,** *18* (11), 7282-7288.
41. Clarke, M. T.; Viscomi, F. N.; Chamberlain, T. W.; Hondow, N.; Adawi, A. M.; Sturge, J.; Erwin, S. C.; Bouillard, J.-S. G.; Tamang, S.; Stasiuk, G. J., Synthesis of super bright indium phosphide colloidal quantum dots through thermal diffusion. *Communications Chemistry* **2019,** *2* (1), 36.
42. Stöber, W.; Fink, A.; Bohn, E., Controlled growth of monodisperse silica spheres in the micron size range. *J. Colloid Interface Sci.* **1968,** *26* (1), 62-69.
43. Graf, C.; Vossen, D. L. J.; Imhof, A.; van Blaaderen, A., A General Method To Coat Colloidal Particles with Silica. *Langmuir* **2003,** *19* (17), 6693-6700.
44. Fu, R.; Jin, X.; Liang, J.; Zheng, W.; Zhuang, J.; Yang, W., Preparation of nearly monodispersed Fe3O4/SiO2 composite particles from aggregates of Fe3O4 nanoparticles. *J. Mater. Chem.* **2011,** *21* (39), 15352-15356.
45. Piao, Y.; Burns, A.; Kim, J.; Wiesner, U.; Hyeon, T., Designed Fabrication of Silica-Based Nanostructured Particle Systems for Nanomedicine Applications. *Adv. Funct. Mater.* **2008,** *18* (23), 3745-3758.

46. Greben, M.; Khoroshyy, P.; Liu, X.; Pi, X.; Valenta, J., Fully radiative relaxation of silicon nanocrystals in colloidal ensemble revealed by advanced treatment of decay kinetics. *J. Appl. Phys.* **2017,** *122* (3), 034304.
47. Jakob, M.; Javadi, M.; Veinot, J. G. C.; Meldrum, A.; Kartouzian, A.; Heiz, U., Ensemble Effects in the Temperature-Dependent Photoluminescence of Silicon Nanocrystals. *Chemistry - A European Journal* **2019,** *25* (12), 3061-3067.
48. Sugimoto, H.; Furuta, K.; Fujii, M., Controlling Energy Transfer in Silicon Quantum Dot Assemblies Made from All-Inorganic Colloidal Silicon Quantum Dots. *J. Phys. Chem. C* **2016,** *120* (42), 24469-24475.
49. Furuta, K.; Fujii, M.; Sugimoto, H.; Imakita, K., Energy Transfer in Silicon Nanocrystal Solids Made from All-Inorganic Colloidal Silicon Nanocrystals. *J. Phys. Chem. Lett.* **2015,** *6* (14), 2761-2766.

TOC graphic